J Mater Sci: Mater Electron (2017) 28:6572–6582
DOI 10.1007/s10854-017-6347-2

Effects of anisotropy of tin on grain orientation evolution in Pb-free solder joints under thermomechanical stress

Jing Han[1] · Fu Guo[1] · Jianping Liu[1]

Received: 7 November 2016 / Accepted: 3 January 2017 / Published online: 11 January 2017

Abstract In this paper, the grain orientation evolution of Pb-free solder joints during thermomechanical fatigue (TMF) was characterized quantitatively using in-situ electron backscattered diffraction (EBSD) observation, which was an effective way to clarify the mechanism of recrystallization. The results showed that the grain orientation evolution of solder joints was significantly affected by the anisotropy of β-tin grains. Recrystallization behavior of a solder joint during TMF was very sensitive to the location of grain boundaries and orientations in the joints. Substantial stress could build up at grain boundaries in real joints in micro-electronic applications under thermomechanical stress, leading to premature failures. Also, slip systems were clarified playing an important role in recrystallization and could be used to predict the subgrain and recrystallized grain formation. While it was conventional cognitive, tricrystals were less likely to develop cracks during TMF and had longer lifetime than single-crystal joints. However, for the tricrystal joint with particularly undesirable orientations, it was clarified that (1 0 1)[1 0 $\bar{1}$] and (1 0 1)[$\bar{1}$ 0 1] silp systems were activated in tricrystals and premature failures occurred with the internal stress caused by anisotropic thermomechanical responses.

1 Introduction

The overall performance of solder joints is dictated by the properties of tin because Pb-free SnAgCu solder joints are mainly comprised of β-tin [1]. The anisotropy of tin is associated with its crystallographic directions and significant variations in its coefficient of thermal expansion (CTE) and elastic modulus. At 298 K, the tin crystals have a body-centered-tetragonal (BCT) structure with lattice parameters of $a_{[100]} = b_{[010]} = 0.5632$ nm and $c_{[001]} = 0.3182$ nm [2]. It has been reported that an extremely strong anisotropy is exhibited in a small Pb-free solder joint which generally comprised one or three grains [3, 4] and substantial strains may develop at grain boundaries of Pb-free solder joints under TMF. As a matter of fact, different joints have different damage evolution behaviors even if they are subjected to the same thermomechanical history because crystallographic orientation arising from solidification processes varies from joint to joint. As a result, the anisotropic property of tin can significantly affect the reliability of Sn-rich solder joints under TMF and may even lead to premature failures of solder joints if these grains have unfavorable orientations. Therefore, grain crystallographic orientations need to be characterized in order to have a better understanding of thermomechanical responses of Pb-free solder joints.

Electronic packages are frequently subjected to temperature variations caused by power on/off switches and environmental change. The microstructure and crystallographic orientations of Pb-free solder joints are not stable during TMF and recrystallization will occur due to the imposed thermalmechanical strain [5, 6]. The recrystallization behavior of solder joints under thermal cycling tests has been extensively studied in the past few years [5–7]. It has been reported that recrystallization in Pb-free solder joints has occurred at locations of large strain gradients [7], but little is known about how this process develops or how it depends on crystal orientations. To assess the intrinsic thermal expansion effects on the

✉ Jing Han
hanjing@bjut.edu.cn

[1] College of Materials Science and Engineering, Beijing University of Technology, Beijing 100124, China

internal stress arising from the anisotropic thermal and elastic properties of tin, finite element analysis was used [8]. Telang et al. attributed the recrystallization and grain growth of a single shear lap solder joint under TMF to the release of elastic strain energy [9]. However, much less work has been done to characterize the microstructural and orientation evolution in the tin phase [10] and the grain orientation information is often neglected in studying the deformation behavior and failure modes of Pb-free solder joints. Moreover, in recent years, the reliability of Pb-free solder joints has been extensively studied and most researchers have focused on the formation and evolution of the intermetallic compounds (IMCs) [11–13], especially near the interface where strain energy is high [12, 13]. However, cracks were constantly observed in the solder bulk in TMF [14, 15]. Some researchers have summarized the effect of the anisotropy in thermal expansion and elastic properties of tin on the significant stress propagation at Sn grain boundaries under TMF, which may result in damage through sliding or decohesion along grain boundaries [15, 16]. Moreover, the actual stress and strain distribution of a solder joint mainly comprised of Sn should be estimated by considering the details of Sn crystallographic orientations in finite element modeling [17].

Microstructural evolution of each joint under thermal fatigue occurred mostly from continuous recrystallization is unique due to the interaction between local thermal and displacement boundary conditions and the significant anisotropic properties of tin grains. However, the effect of anisotropic nature of tin on thermal fatigue lives of SnAgCu Pb-free joints has not yet been fully discussed and in-situ EBSD observation has not been used in prior studies [14–16]. For a better understanding of the reliability and to identify the failure mechanism of Pb-free solder joints, it is significant to understand the relationship between the crystallography of tin and the failure process in the joints using in-situ EBSD observation.

In this paper, SnAgCu solder joints in electronic packages have been subjected to TMF within the temperature range of 273–373 K and failures have been observed. Orientation imaging microscopy (OIM) was used to obtain crystallographic information to provide a detailed characterization of the damage evolution in solder joints under TMF. And the significant effect of anisotropy of tin on thermal fatigue lives of solder joints has been observed in real SnAgCu Pb-free solder joints in micro-electronic applications using in-situ EBSD observation. The results suggest that substantial stress can build up at grain boundaries in real joints in micro-electronic applications under TMF and these grains failed earlier if they had unfavorable orientations. The in-situ EBSD observations and analysis described in this paper provides a better understanding of effects of anisotropy of tin on microstructure and damage evolution of Pb-free solder joints under thermomechanical stress.

2 Experimental

Chip scale packaged ball grid arrays (BGA) with 228 solder bumps in 0.5 mm pitch were used in this study. The composition of the solder bump was Sn3.0Ag0.5Cu. The package dimension was 12 mm × 12 mm × 1.1 mm and the solder bump size was 300 μm in diameter. The BGA packages were soldered onto the non-solder mask defined Cu pad of a FR-4 printed circuit board using a typical reflow profile. The peak temperature of the reflow profile was 518 K and the duration at temperature above 490 K was 1 min. The X-ray transmission image of a Sn3.0Ag0.5Cu BGA package is shown in Fig. 1. The specimens without mounting in epoxy were cross-sectioned, ground with SiC papers and then polished with diamond suspensions to obtain the original crystal orientation of the solder joints. It was essential to perform the final polishing carefully with 0.05 μm colloidal silica suspension. Due to the birefringent properties of Sn, different orientations of Sn grains can be observed as different colors under cross-polarized light. As a result, grain orientations in solder joints were characterized quickly by the optical microscopy with cross-polarized light.

The BGA assemblies were then subjected to TMF within the temperature range of 273–373 K. The dwell time at each temperature extreme was 15 min and the ramp rate was about 100 K/min. The same location of the same specimen was scanned after 2000 TMF to obtain the changes and similarities in the orientations.

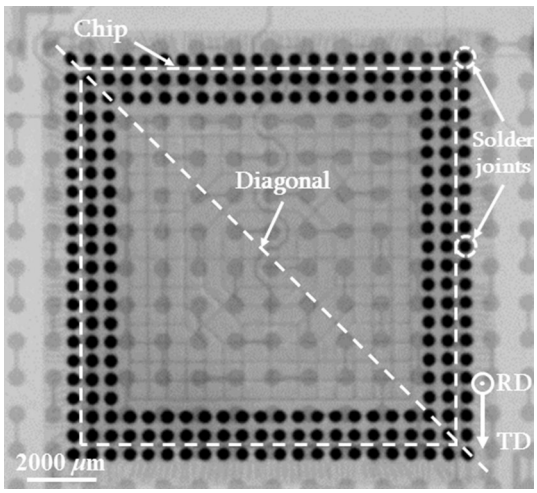

Fig. 1 X-ray transmission image of Sn3.0Ag0.5Cu BGA packages employed in the TMF within the temperature range of 273–373 K

Due to complex functions of heat, water vapor and air, the surface of the cross-section was contaminated after TMF and the indexing of EBSD patterns became very difficult. Therefore, cross-sectioned joints were encapsulated in a glass tube to eliminate the inability of pattern indexing from the cross-section contamination after TMF.

The crystallographic orientation details of the solder joints were characterized quantitatively by EBSD. The OIM data was collected by OIM Data Collection 5.2 software (TexSEM Laboratories, Inc., UT, USA) using a 30 kV beam. The obtained datasets were one time cleaned-up by incorporating lower confidence index points with higher confidence index points using a nearest neighbor correlation technique. Pixels with low confidence of correct indexing were switched to the orientation of a neighboring pixel with a high confidence and the small Cu_6Sn_5 and Ag_3Sn IMCs particles were removed from the orientation maps. Black areas on maps represent unindexed orientations.

3 Results

Figure 2a, c show the EBSD orientation map and the (001) and (100) pole figures of the cross-section of a single-grained as-reflowed solder joint, respectively. Figure 2a also shows the grain boundary distribution of calculated misorientation angles that range from 2° to 180° and red lines are defined as those with misorientations less than 5°. Figure 2b shows misorientation histograms of the joint in Fig. 2a, illustrating the presence of low-angle boundaries up to about 5°. As shown in Fig. 2, the joint was typically composed of one grain which had the c-axis nearly parallel (15°) to the pad.

Figure 3a, c show the EBSD orientation map (with the grain boundary distribution) and the (001) and (100) pole figures of the cross-section of a bicrystal as-reflowed solder joint, respectively. High angle grain boundaries indicated with blue lines are defined as those with misorientations more than 15°, while red and green lines denote for misorientations less than 5° and misorientations between 5° and 15°, respectively. Figure 3b shows

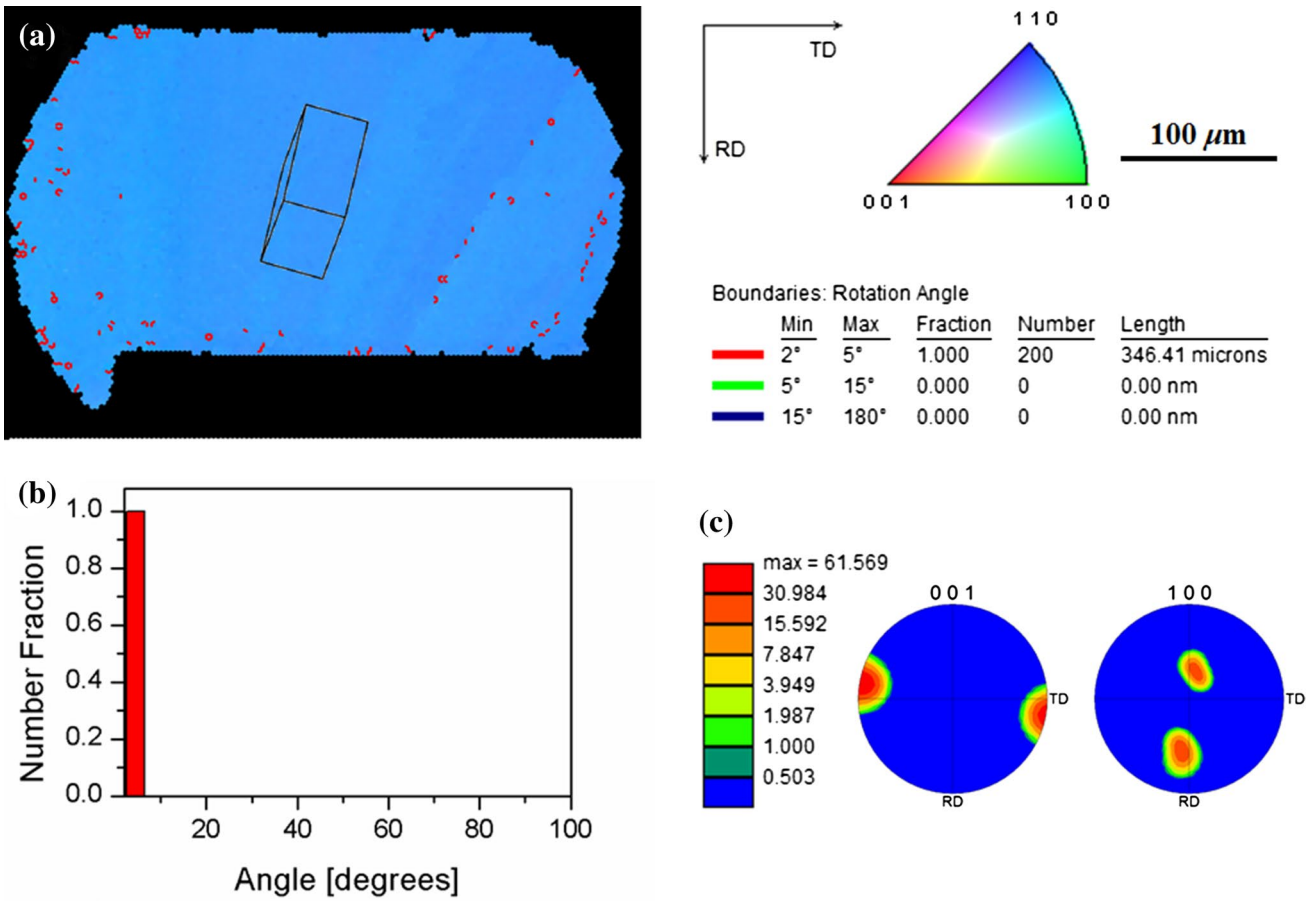

Fig. 2 A single-grained as-reflowed Sn3.0Ag0.5Cu solder joint **a** EBSD orientation map of the joint(with grain boundary distribution), **b** misorientation histograms of the joint, **c** (001) and (100) pole figures of the joint

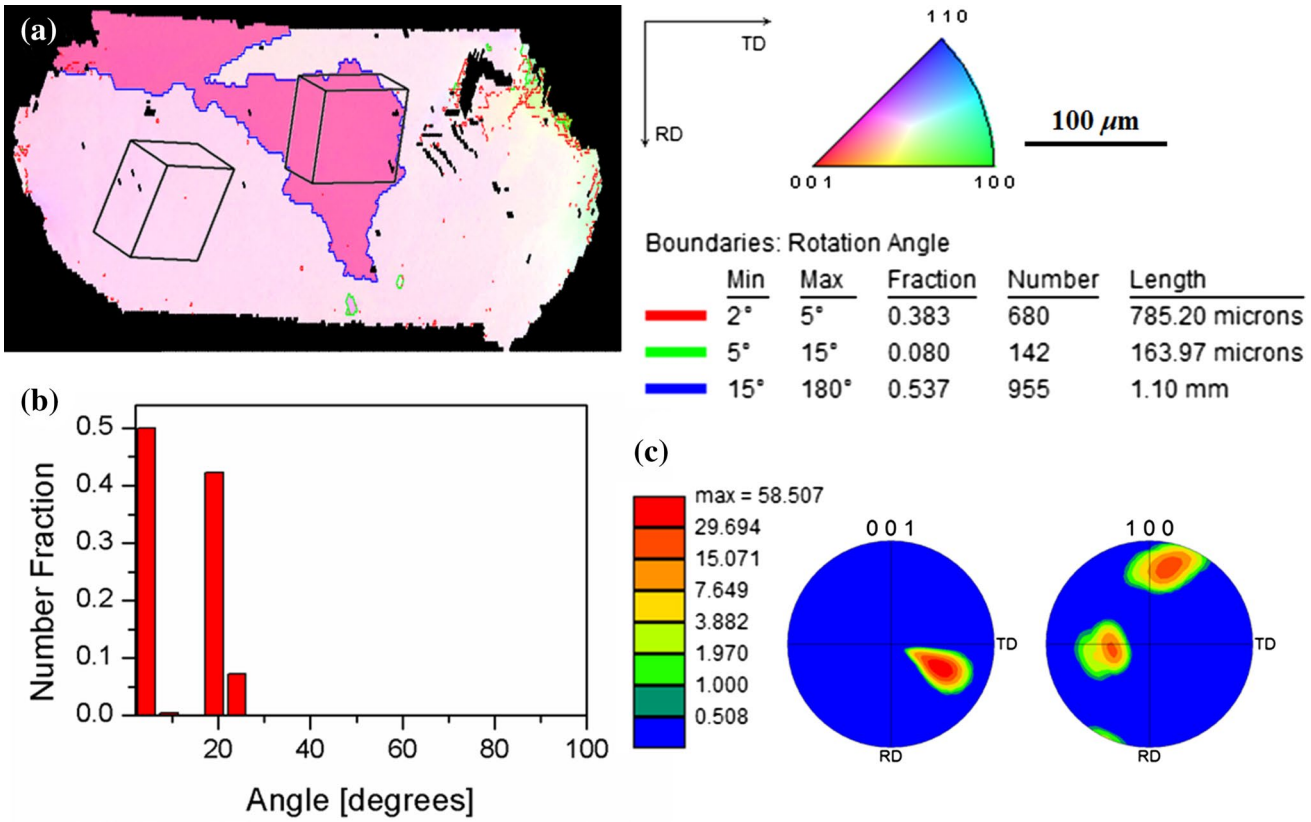

Fig. 3 A bicrystal as-reflowed Sn3.0Ag0.5Cu solder joint **a** EBSD orientation map of the joint(with grain boundary distribution), **b** misorientation histograms of the joint, **c** (001) and (100) pole figures of the joint

misorientation histograms of the joint in Fig. 3a, illustrating the presence of low-angle boundaries up to about 10° and misorientations in the range of 15°–25°. As shown in Fig. 3, the joint was typically composed of two grains.

Figure 4a, c show the EBSD orientation map and the (001) and (100) pole figures of the cross-section of an as-reflowed solder joints with tricrystals, respectively. Figure 4b shows the misorientation histograms of the solder joint, illustrating the presence of low-angle boundaries up to about 15° and twin misorientations in the range of 55°–65°. This range of angles reflects the presence of two twin orientation relationships. There is a 57.2° ⟨100⟩ rotation or a 62.8° ⟨100⟩ rotation in tricrystals [18, 19]. The fact that these angles are close to 60° implies that low-angle boundaries, orientation gradients, and/or grain boundary dislocations can accommodate a few degrees of mismatch to make large tricrystals (three orientations, shown in Fig. 4c). Both types of twin boundary can exist, as evident in Fig. 4b, leading to a double peak, which can compensate for the nonperfect 60° misorientation. It can be clearly seen from the misorientation histograms, the misorientation distribution function (MDF) and the grain boundary map (see Fig. 3a, b) that the three grains are twin-related with about 60° rotation about the [100] axis. The result is in good agreement with those obtained in previous studies [18–20].

Figure 5a–c show the EBSD orientation map, the misorientation histograms and the (001) and (100) pole figures of the cross-section of an as-reflowed solder joint, respectively. As shown in Fig. 5a, c it seems that the joint is composed of two grains, as there are strong peaks for only two (001) poles for bicrystal orientations with a common [100] axis. However, Fig. 5b shows misorientation histograms and MDF of the cross-section of the solder joint, illustrating the presence of low-angle boundaries up to about 10° and twin misorientations in the range of 55°–65° with a rotation about [100] axis. Therefore, it was reasonable to assume that the joint was composed of tricrystals presenting two types of twin misorientations in the range of 55°–65°. Meanwhile, further polishing may result in complete removal of grain boundaries and thus reveal completely different orientations and microstructures of the solder joints, which is considered as the reason that in-situ EBSD observation should be used to investigate the recrystallization behavior and the grain orientation evolution of Pb-free solder joints under thermomechanical stress.

Figure 5d represents the EBSD orientation map of the cross-section of the same as-reflowed solder joint shown

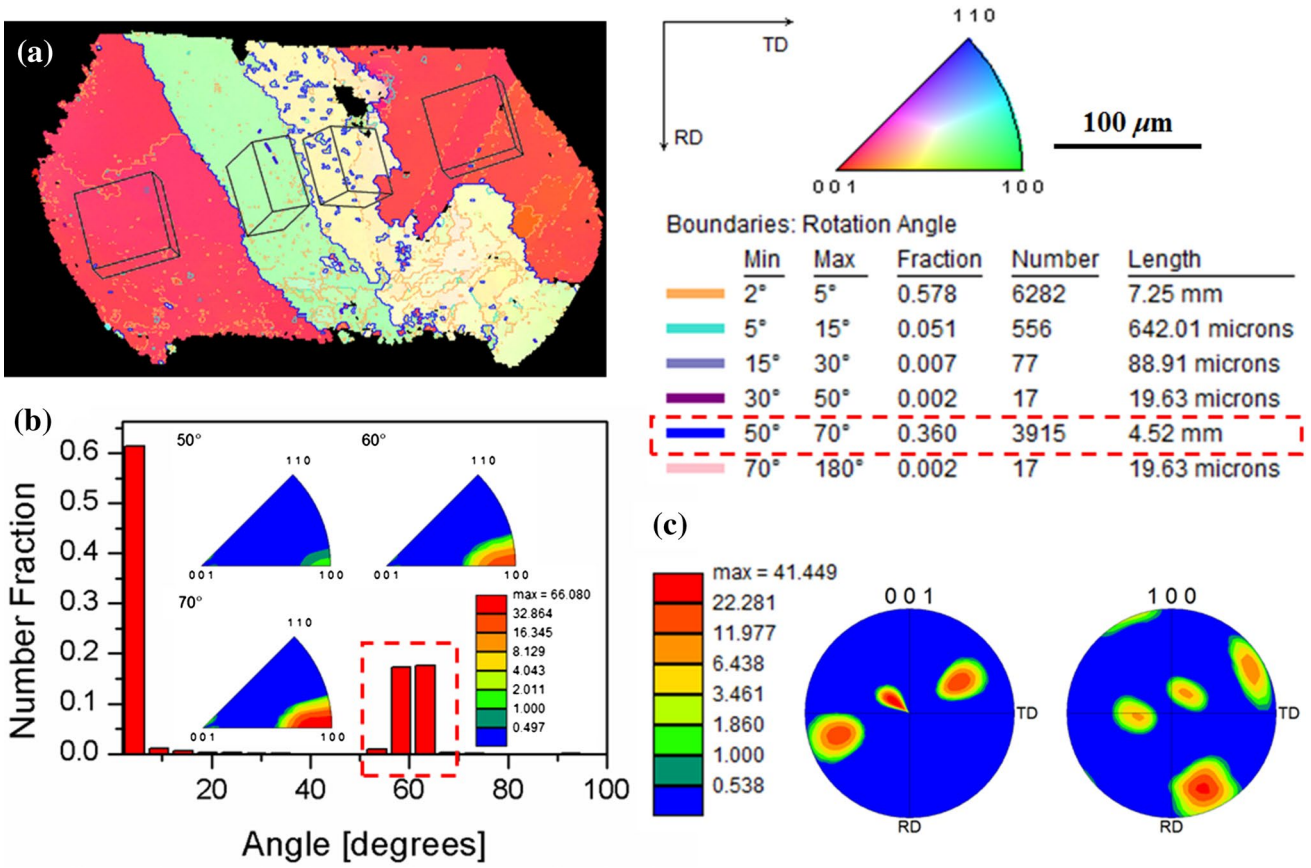

Fig. 4 Twin orientations in a tricrystal as-reflowed Sn3.0Ag0.5Cu solder joint(cyclic twin relationship with near 60° rotations about a common [100] axis) **a** EBSD orientation map of the joint(with grain boundary distribution), **b** misorientation histograms and MDF of the joint, **c** (001) and (100) pole figures of the joint

in Fig. 5a after further polishing. As shown in Fig. 5d, the joint was typically composed of tricrystals. Figure 5e, f show the misorientation histograms and the (001) and (100) pole figures of the cross-section of the as-reflowed solder joint, respectively. As shown in Fig. 5e misorientation histograms and MDF of the cross-section of the solder joint illustrated the presence of low-angle boundaries up to about 10° and twin misorientations in the range of 55°–65°, which demonstrated tricrystals existing in the Sn3.0Ag0.5Cu solder joint. Therefore, it was reasonable to assume that a joint presenting two-grained with twin misorientations in the range of 55°–65° with a common [100] axis was composed of tricrystals.

Figure 6a shows the EBSD orientation map of the cross-section of a single-grained as-reflowed solder joint locating at the corner of a package for in-situ EBSD observation; Fig. 6c shows the (001) and (100) pole figures of the cross-section of the joint. As shown in Fig. 6a, c, the joints were typically composed of one grain. Figure 6b shows misorientation histograms of the joint in Fig. 6a, illustrating the presence of low-angle boundaries up to about 5°. After 2000 TMF between 273 K and 373 K, the cross-section of the corner joint in the exterior row revealed recrystallization, as shown in Fig. 6d. EBSD orientation map and (001) and (100) pole figures of the solder joint shown in Fig. 6a after 2000 TMF are shown in Fig. 6d, f respectively. With 2000 TMF, the streaks became wider, indicating spreading of the crystal orientations. Figure 6e shows misorientation histograms of the joint, illustrating the presence of low-angle boundaries up to about 15°. The discrete pole figure in Fig. 6f and the misorientation histograms in Fig. 6e reflect the presence of orientation gradients in that the pole has an angular spread of about 5°–15°.

Figure 7a, c show the EBSD orientation map and the (001) and (100) pole figures of a cross-section of an as-reflowed solder joints with tricrystals, respectively. Figure 7b shows misorientation histograms and MDF of the solder joint, illustrating the presence of low-angle boundaries up to about 10° and twin misorientations in the range of 55°–65°. Figure 7d, f show the EBSD orientation map and the (001) and (100) pole figures of the

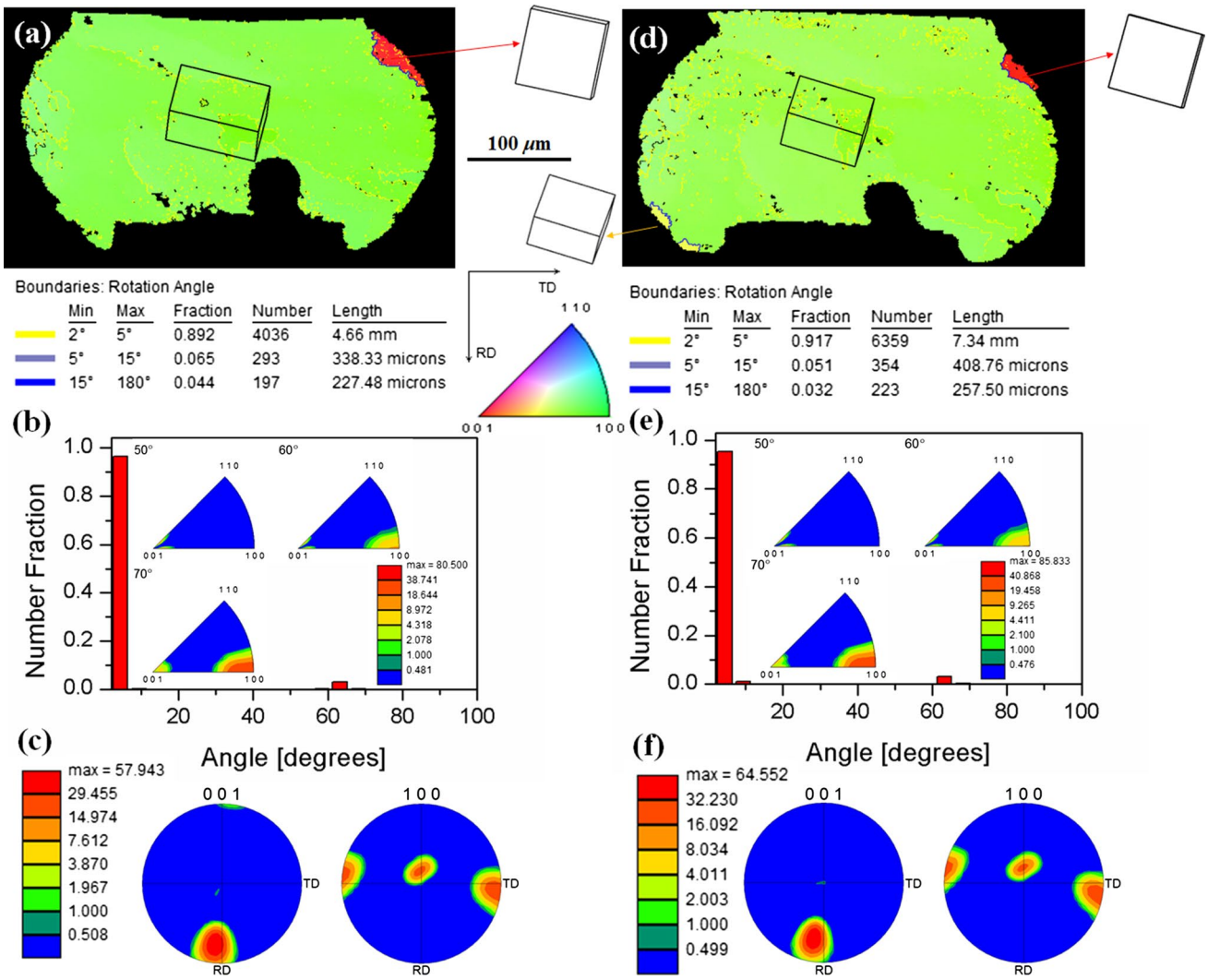

Fig. 5 **a** EBSD orientation map of a cross-section of an as-reflowed Sn3.0Ag0.5Cu solder joint and a schematic reflecting the Sn orientations, **b** misorientation histograms and MDF of the cross-section shown in (**a**), **c** (001) and (100) pole figures of the cross-section shown in (**a**), **d** EBSD orientation map of the cross-section of the as-reflowed Sn3.0Ag0.5Cu solder joint shown in (**a**) with further polishing (cyclic twin relationship with near 60° rotations about a common [100] axis) and a schematic reflecting the Sn orientations, **e** misorientation histograms and MDF of the cross-section shown in (**d**), **f** (001) and (100) pole figures of the cross-section shown in (**d**)

cross-section shown in Fig. 7a after 2000 TMF, respectively. The discrete pole figure in Fig. 7f also reflects the presence of orientation gradients in that the pole has an angular spread of about 5°–30°. There were many small grains with varied colors in the localized regions and each color represented an orientation. The orientations of the small grains were different from those of the grains in as-reflowed solder joints. The sizes of the small equiaxed grains with various orientations ranged from 5 to 30 μm, which indicated that the localized recrystallization occurred in the Pb-free solder joint. The results agreed well with those obtained in previous studies [9, 10].

4 Analysis and discussion

4.1 Grain orientations of as-reflowed Pb-free solder joints

Although each as-reflowed Pb-free BGA solder joint had its unique orientation characteristics, the joints were typically composed of only one or three grains. EBSD orientation maps of cross-sections of 300 as-reflowed solder joints were taken and investigated. A total of 176 joints of them are composed of only one grain, which is in good agreement with the results obtained in the previous studies [10, 14, 15], while others are composed of two to four

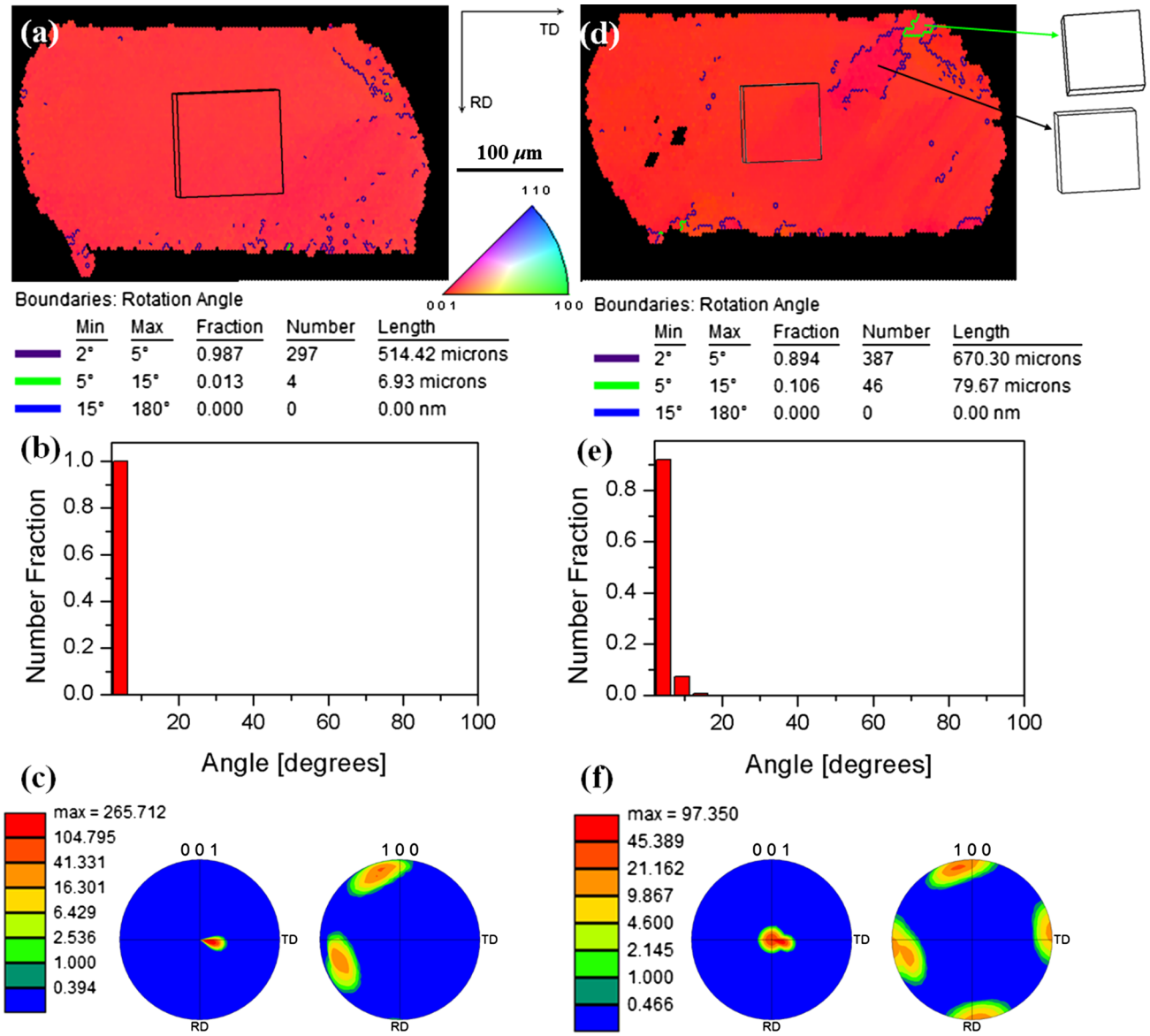

Fig. 6 **a** EBSD orientation map of a single-grained as-reflowed Sn3.0Ag0.5Cu solder joint for in-situ observation, **b** misorientation histograms of the joint shown in (**a**), **c** (001) and (100) pole figures of the joint shown in (**a**), **d** EBSD orientation map of the joint shown in (**a**) after 2000 TMF between 273 K and 373 K, **e** misorientation histograms of the joint shown in (**d**), **f** (001) and (100) pole figures of the joint shown in (**d**)

grains 80 percent of them are tricrystals (where there is a 57.2° ⟨010⟩ rotation or a 62.8° ⟨010⟩ rotation [18, 19]). During the as-reflowed process, due to the high entropy of fusion of BCT Sn (14 J/mol K) [19, 21, 22], more latent heat of freezing is released, and the nucleation of the Sn grains is suppressed. Meanwhile, for Sn and Sn-rich solder alloys, Sn dendrites grow fast due to the significant undercooling. Therefore, there are typically a few grains in the solder joints [23], and twin boundaries (stacking faults) with low-energy are likely to form in the as-reflowed solder joints [18, 19].

At 303 K, α [100] = α [010] = 16.5×10^{-6} K^{-1}, α [001] = 32.4×10^{-6} K^{-1} and α_{Cu}=16.6×10^{-6} K^{-1} [24, 25]. Therefore, the CTE mismatch is the highest possible value when the c axis is nearly parallel to the Cu pad (the joint was in tension at high temperatures). If considering the variation of CTE by temperature, the conclusion is tenable [24]. Therefore, in order to investigate the microstructure evolution of Pb-free solder joints under thermo-mechanical stress, the anisotropic property of Pb-free solder joints affected by the anisotropic property of Sn and

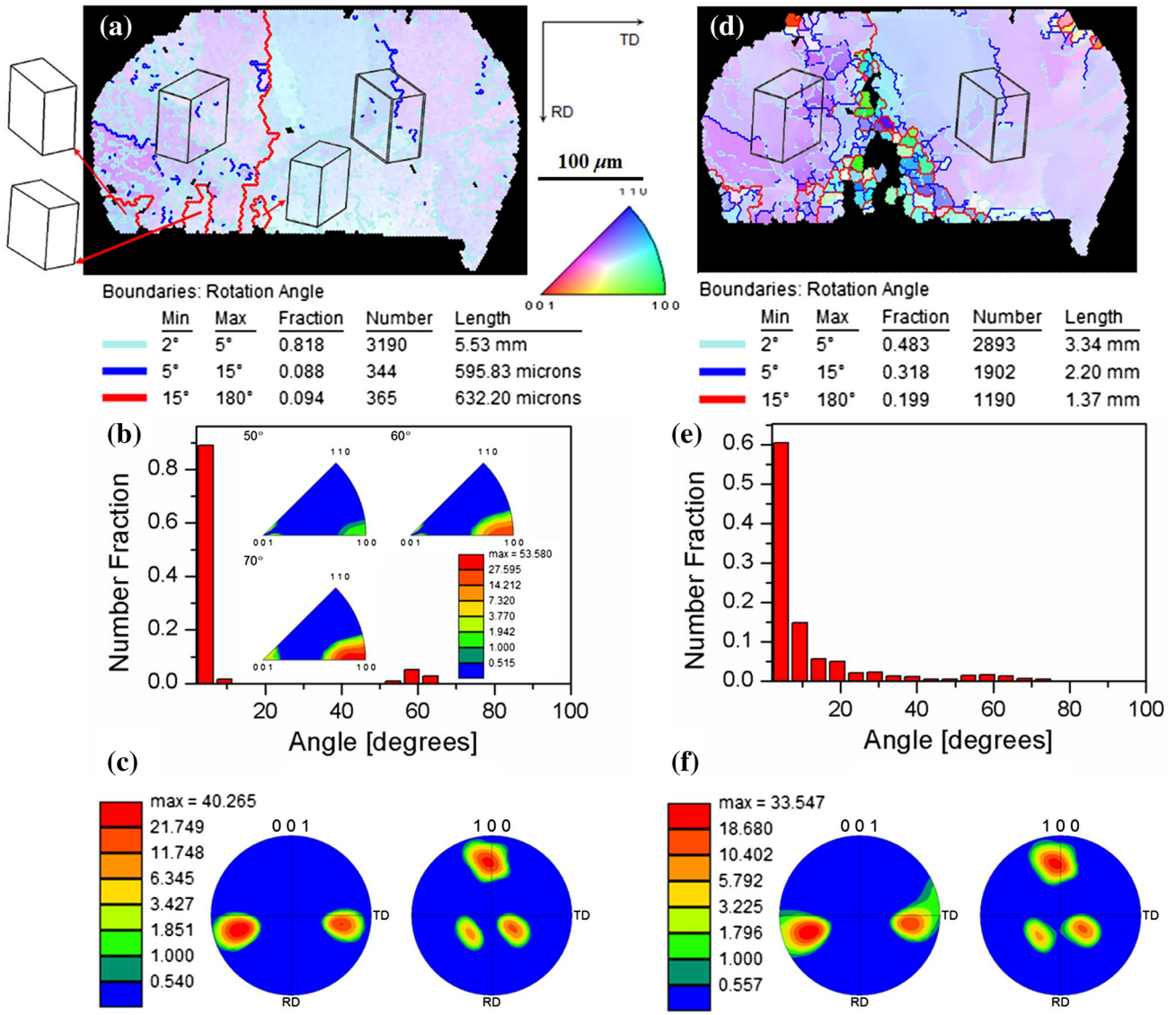

Fig. 7 **a** EBSD orientation map of a tricrystal as-reflowed Sn3.0Ag0.5Cu solder joint for in-situ observation, **b** misorientation histograms and MDF of the joint shown in (**a**), **c** (001) and (100) pole figures of the joint shown in (a); **d** EBSD orientation map of the joint shown in (**a**) after 2000 TMF between 273 K and 373 K, **e** misorientation histograms of the joint shown in (**d**), f (001) and (100) pole figures of the joint shown in (**d**)

the small amount of grain numbers and orientations in Pb-free solder joints should be taken into consideration.

4.2 Recrystallization behavior of a single-grained as-reflowed joint

During TMF, for a single-crystal as-reflowed solder joint, strains develop because of the differential thermal expansion constraint by the package and pad on the joint. Therefore, every joint contains only one grain is a special case with a different detailed deformation history [26]. Recrystallization occurred at corners in the exterior row where extrinsic shear strains arising from CTE mismatch were largest. As strain accumulates within a given grain, dislocations were absorbed (recover) in low-angle boundaries, leading to gradual increases in the subgrain misorientation by continuous recrystallization [10]; once the misorientation exceeded about 15°, they were no longer considered subgrains. Furthermore, in situ EBSD maps showed much more orientation spreading and emergence of new orientations in diffraction patterns after 4000 TMF, which would be described in more detail in a future paper.

β-tin crystals have an anisotropic BCT structure with c/a = 0.546. At 303 K, the CTEs in the principal directions are α [100] = α [010] = 16.5×10^{-6} K^{-1} and α [001] = 32.4×10^{-6} K^{-1}, respectively, and the values

change substantially at high temperatures. For instance, at 403 K, the CTEs in the principal directions are α [100] = α [010] = 20.2×10^{-6} K^{-1} and α [001] = 41.2×10^{-6} K^{-1}, respectively [24, 25]. During TMF, localized stress between orientations and the pads caused by the CTE mismatch between orientations with the c-axis nearly parallel to the pad was higher than that between orientations with the c-axis nearly perpendicular to the pad. So for single-crystal joints, cracks developed facilely between the orientations with the c-axis nearly parallel to the pad during TMF. Therefore, assuming that a random distribution of grain orientations presents in a package, the axial displacement history of the package with respect to the pad will be close to the average expansion value of Sn. The expansion coefficient of joints with the c axis parallel to the board is the lowest possible value in the basal plane, and these joints will be in tension at high temperatures. While joints that have the c-axis perpendicular to the board will be in compression at high temperatures.

The recrystallized grain orientations have different orientations from the original crystal, therefore, for each newly recrystallized grain, there are different expansion rates in the board-normal direction [24, 25]. During each TMF, gradual changes will be made in the local stress state, and there can be an increase or a decrease in the magnitude of the local stress in newly recrystallized grains. Formation of any other orientation in grains with the c-axis nearly parallel (1.5°) to the pad shown in Fig. 6 will have the effect of reducing the tensile stress, and there will be a reduction in the local strain energy and dislocation activity. The elastic strain energy in a grain can reduce and the local stress state along grain boundaries increases after the formation of a new orientation, therefore, the dislocation activity and grain boundary sliding contributing to the damage nucleation will facilitate [24, 26].

4.3 Recrystallization behavior of a tricrystal as-reflowed joint

After 2000 TMF, for the joint locating at the corner of the package, recrystallization behavior was observed at the corner of the joint as shown in Fig. 6d. However, of 22 joints in the exterior row of the package, the joint which were tricrystal orientations locating in the middle (the 11th) of the edge had large area recrystallization and cracks (14 joints in the exterior row were single-crystal, while 7 other joints were tricrystal. None of which cracked.). Low angle boundaries were often observed within a large grain section that could compensate for the nonperfect 60° angles required for the hexagonal microstructure features and there was a percolative path along the crack dominating by grain boundaries. This was a consequence of the anisotropic properties of Sn that caused exaggerated and irregular deformation arising from tricrystal grain microstructures [24, 26, 27].

The stress evolution in a joint is complex and varies locally with the grain boundary geometry due to the anisotropic of Sn [13, 14]. And the stress history in a solder joint is unique because of the interaction between the thermal-displacement boundary conditions arising from the position of the joint in the array and the crystal orientations and grain misorientations. For tricrystals, internal strains develop due to the differential thermal expansion constraint by the package and pad on the joint, and due to the intrinsic anisotropic expansion of Sn during TMF. Grain boundary sliding, dislocation creep, and plastic deformation occur due to the sufficient stress caused by oscillating internal strains during TMF [24, 26, 27]. Knowledge of activated slip systems can be used to predict subgrain boundary formation because dislocation slip is the direct cause of continuous recrystallization. Therefore, the clarification of activated slip systems during TMF is necessary to further understand the recrystallization process of solder joints.

There are 15 common nonequivalent slip systems in Sn and (1 0 1)[0 1] has the lowest ideal shear resistance among the 15 slip systems [28]. During TMF, the activation of slip systems depended on crystal orientation, and for grains shown in Fig. 7a, the probable slip systems were (1 0 1)[1 0 $\bar{1}$] and (1 0 1)[$\bar{1}$ 0 1], respectively. Therefore, the stress activated the main (1 0 1)[$\bar{1}$ 0 1] group of slip systems and the joint with tricrystals in the middle of the exterior row of the package exhibited recrystallization, which was well developed than those found in the joint with orientations with the c-axis parallel to the pad in the corner of the package. These preliminary observations also show that there is solidification microstructure for cyclic strain where even tricrystal orientations cannot resist damage accumulation. The diffraction pattern shows much more extensive streaks for the tricrystals, indicating the presence of substantial orientation gradients, low-angle boundaries and new orientations. Therefore, we can assume that different kinds of distributions of grain boundaries and orientations inhibit dislocation glide and lead to dislocations recovering at different rates to form subgrain boundaries gradually increasing in misorientations. This confirms the anisotropy of thermomechanical responses of grains with different orientations in Pb-free solder joints. Therefore, the grain orientation has a great effect on the damage generation and subsequent failure modes and it indicates the recrystallized grains prefer to nucleate along the pre-existing high-angle grain boundaries.

During TMF, large stress developed at the original grain boundary and the displacement of original grains was not uniform due to coefficient of thermal expansion mismatch of β-tin grains with different orientations [24, 27]. As a result, the large CTE mismatch between the two

original twin-oriented grains led to the subsequent facilitated recrystallization. Therefore, a twin grain boundary (coincided with a high stress concentration area) would accelerate the initiation and propagation of cracks or change the cracking path and corresponding failure mode, leading to the fast degradation and premature failure of solder joints. This is not consistent with the results obtained from other literatures (Joints with the c-axis parallel to the pad or with multiple orientations are less likely to develop an axial tensile stress that facilitates fracture, because they have effective CTE values closer to the average CTE) [9, 10]. Thus, it is not yet possible to address reliability prediction of Sn-based solder joints in a physically satisfying way, because the deformation behavior of Sn evolves in complex ways that can only be understood if its anisotropic properties can be incorporated into predictive models in quantifiable ways.

5 Conclusion

In this paper, a Sn3.0Ag0.5Cu ball grid array package was investigated and the significant effect of the crystallographic anisotropy of Sn grains on recrystallization and damage evolution in TMF treatment of Sn3.0Ag0.5Cu solder joints was discussed. In order to precisely investigate the influence of anisotropic thermomechanical responses of Sn on the damage evolution in Pb-free solder joints under TMF, in-situ EBSD observation was used to investigate the grain orientation evolution in this paper. The tricrystal Sn3.0Ag0.5Cu solder joint in micro-electronic applications shows premature damages, indicating the great effect of anisotropy of tin on the damage generation of solder joints by grain boundary sliding. Furthermore, it also has a great effect on subsequent failure mode of solder joints and may result in a catastrophic failure of solder joint with the internal stress caused by anisotropic thermomechanical responses. The internal stress will make cracks initiate and propagate in Pb-free solder joints more facilely under TMF, leading to fast degradation and premature failure of solder joints. If a high angle grain boundary coincides with a high stress concentration area, the initiation and propagation of cracks will be accelerated or the cracking path and corresponding failure mode will be changed. There is clearly an interrelationship between the grain orientations and the process of recrystallization, which needs to be addressed and understood quantitatively before prediction of joint lifetimes can be accomplished on the basis of physically understood and modeled mechanisms. This is clearly possible, as control of microstructural evolution is a common outcome of focused metallurgical research for production of high-volume products. But with regard to reliability prediction, it is more important to understand the deformation and recrystallization processes that govern the most vulnerable crystal orientations with respect to their time-temperature-displacement history. Moreover, based on in-situ EBSD observation, our next work is to calculate rotation angles and axes of recrystallized grains from parent crystals. Also, in our future studies, dislocation and slip systems should be described in more detail to further understand the recrystallization process in Pb-free solder joints.

Acknowledgements This work was supported by the National Natural Science Foundation [Grant Number 51401006], the Beijing Natural Science Foundation [Grant Numbers 2162005 and 2172009] and the Science and Technology Project of Beijing Municipal Education Commission [Grant Number KM201710005003].

References

1. P. Darbandi, T.R. Bieler, F. Pourboghrat, T.K. Lee, J. Electron. Mater. **43**, 2521–2529 (2014)
2. T.-K. Lee, B. Zhou, L. Blair, K.C. Liu, T.R. Bieler, J. Electron. Mater. **39**, 2588–2597 (2010)
3. B. Zhou, T.R. Bieler, T.K. Lee, K.C. Liu, J. Electron. Mater. **39**, 2669–2679 (2010)
4. B. Zhou, G. Muralidharan, K. Kurumadalli, C.M. Parish, S. Leslie, T.R. Bieler, J. Electron. Mater. **43**, 57–68 (2014)
5. T.T. Mattila, J.K. Kivilahti, IEEE Trans. Compon. Packag. Technol. **33**, 629–635 (2010)
6. A. Mayyas, A. Qasaimeh, P. Borgesen, M. Meilunas, Microelectron. Reliab **54**, 447–456 (2014)
7. B. Zhou, T.R. Bieler, T.K. Lee, W.J. Liu, J. Electron. Mater. **42**, 319–331 (2013)
8. P. Darbandi, T.R. Bieler, F. Pourboghrat, T.K. Lee, J. Electron. Mater. **42**, 201–214 (2013)
9. A.U. Telang, T.R. Bieler, A. Zamiri, F. Pourboghrat, Acta Mater **55**, 2265–2277 (2007)
10. T.K. Lee, C.U. Kim, T.R. Bieler, J. Electron. Mater. **43**, 69–79 (2014)
11. H.Y. Hsiao, C.M. Liu, H.W. Lin, T.C. Liu, C.L. Lu, Y.S. Huang, C. Chen, K.N. Tu, Science **336**, 1007–1010 (2012)
12. S.K. Seo, S.K. Kang, M.G. Cho, H.M. Lee, JOM **38**, 22–29 (2010)
13. M.A.A. Mohd Salleha, S.D. McDonalda, H. Yasudac, A. Sugiyamad, K. Nogita, Scr. Metall. **100**, 17–20 (2015)
14. T.R. Bieler, B. Zhou, L. Blair, A. Zamiri, P. Darbandi, F. Pourboghrat, T.-K. Lee, K.-C. Liu, J. Electron. Mater. **41**, 283–301 (2012)
15. B.T. Zhou, Q. Zhou, T.R. Bieler, T.K. Lee, J. Electron. Mater. **44**, 895–908 (2015)
16. M.H. Lu, D.Y. Shih, P. Lauro, C. Goldsmith, D.W. Henderson, Appl. Phys. Lett. **92**, 211909-211909-3 (2008)
17. S.B. Park, R. Dhakal, J. Gao, J. Electron. Mater. **37**, 1139–1147 (2008)
18. L.P. Lehman, S.N. Athavale, T.Z. Fullem, A.C. Giamis, R.K. Kinyanjui, M. Lowenstein, K. Mather, R. Patel, D. Rae, J. Wang, Y. Xing, L. Zavalij, P. Borgesen, E.J. Cotts, J. Electron. Mater. **33**, 1429–1439 (2004)
19. L.P. Lehman, Y. Xing, T.R. Bieler, E.J. Cotts, Acta Mater **58**, 3546–3556 (2010)
20. R. Dudek, R. Doring, B. Michel, ASME Trans. **125**, 562–570 (2003)
21. A.U. Telang, T.R. Bieler, Scripta Mater **52**, 1027–1031 (2005)

22. S. Terashima, M. Tanaka, Sci. Technol. Weld. Join. **14**, 468–475 (2009)
23. D.W. Henderson, J.J. Woods, T.A. Gosselin, J. Bartelo, D.E. King, T.M. Korhonen, M.A. Korhonen, L.P. Lehman, E.J. Cotts, S.K. Kang, P. Lauro, D.Y. Shih, C. Goldsmith, K.J. Puttlitz, J. Mater. Res. **19**, 1608–1612 (2004)
24. M.A. Matin, E.W.C. Cohen, W.P. Vellinga, M.G.D. Geers, Scripta Mater **53**, 927–932 (2005)
25. W.B. Pearson, A handbook of lattice spacings and structure of metals and alloys, vol. 2 (Pergamon, London, 1958)
26. J. Han, S.H. Tan, F. Guo, J. Electron. Mater. **45**, 6086–6094 (2016)
27. S.H. Tan, J. Han, F. Guo, J. Mater. Sci: Mater. Electron. **27**, 9642–9649 (2016)
28. Y. Kinoshita, H. Matsushima, N. Ohno, Modell. Simul. Mater. Sci. Eng. **20**, 35003–35011 (2012)